Published in final edited form as:
J Mol Biol. 2014 September 23; 426(19): 3314–3324. doi:10.1016/j.jmb.2014.07.009.

Adaptive remodelling by FliN in the bacterial rotary motor

Richard W. Branch[a], **Michael N. Sayegh**[a], **Chong Shen**[a,b], **Vedavalli S.J. Nathan**[a,c], and **Howard C. Berg**[a,1]

[a]Department of Molecular and Cellular Biology, Harvard University, Cambridge, MA, USA

Abstract

Sensory adaptation in the *E. coli* chemosensory pathway has been the subject of interest for decades, with investigation focusing on the receptors that process extracellular inputs. Recent studies demonstrate that the flagellar motors responsible for cell locomotion also play a role, adding or subtracting FliM subunits to maximise sensitivity to pathway signals. It is difficult to reconcile this FliM remodelling with the observation that partner FliN subunits are relatively static fixtures in the motor. By fusing a fluorescent protein internally to FliN, we show that there is in fact significant FliN remodelling. The kinetics and stoichiometry of FliN in steady-state and in adapting motors are investigated and found to match the behaviour of FliM in all respects except for timescale, where FliN rates are about four times slower. We notice that motor adaptation is slower in the presence of the fluorescent protein, indicating a possible source for the difference. The behaviour of FliM and FliN is consistent with a kinetic and stoichiometric model that contradicts the traditional view of a packed, rigid motor architecture.

Keywords

Escherichia coli; bacterial motility; signal transduction; sensory adaptation; protein subunit exchange

Introduction

Bacterial flagellar motors in *E. coli* switch between clockwise (CW) and counterclockwise (CCW) rotation[1–3]. The probability of CW rotation (the CW bias) is controlled by the level of the phosphorylated chemotaxis response regulator, CheY-P[4]. The switch complex in the motor is a protein ring composed of subunits of FliG, FliM and FliN[5]. FliG interfaces with

[1]To whom correspondence should be addressed. Address: Harvard University Biolabs, 16 Divinity Avenue, Room 3063A, Cambridge, MA 02138, USA. Phone: 001-617-495-0924. Fax: 001-617-496-1114. hberg@mcb.harvard.edu. .
[b]Present address: Department of Physics, University of Science and Technology of China, Hefei, China
[c]Present address: Department of Genetics, Harvard Medical School, Boston, MA, USA

Contributions R. W. B. and H. C. B. designed research. R. W. B., M. N. S. and C. S. conducted experiments. R. W. B., M. N. S. and C. S. analyzed data. V. S. J. N., R. W. B. and M. N. S. conducted genetic work. R. W. B and H. C. B. wrote the paper.

the motor's torque-generating units at the periphery of the complex[6]. Binding of CheY-P to FliM[7] and FliN[8] promotes conformational changes in FliG that result in CW rotation[9].

Recent studies have identified the ability of the motor to adapt to the steady-state concentration of CheY-P, set by the chemotaxis network[10]. FliM subunits continuously exchange between the motor and the cytoplasm[11]. The details of exchange differ between the rotational states of the motor, such that CCW motors are able to host more subunits than CW motors[12]. When steady-state [CheY-P] is low, the motor spends more time in the CCW state and remodels by adding FliM subunits[10]. With more ligand binding sites present, the motor is able to sense lower levels of CheY-P and bias is partially restored.

We would like to understand how the architecture of the switch complex changes during motor adaptation. Studies have revealed mismatches in the exchange kinetics of FliG, FliM and FliN, raising questions about how remodelling proceeds. FliG appears to be anchored to the motor: fluorescence studies have not observed any exchange of the protein between motor and cytoplasm[13,14]. In fluorescent studies of FliN, ~10% of the protein exchanges in ~1 hr[13]. In comparison, upwards of ~25% of FliM exchanges in ~2 min[12]. This discrepancy between FliM and FliN kinetics is surprising, given the position of FliN at the base of the complex below FliM[5], and its role in binding CheY-P in conjunction with FliM[8]. Here, we re-visit the topic of FliN exchange and investigate its role in motor adaptation.

Results

FliN fluorescent fusions

We investigated the functionality of various FliN fluorescent fusions. The fluorescent protein $eYFP^{A206K}$ (eYFP with alanine at residue 206 substituted for lysine, to prevent aggregation, referred to hereafter as YFP) was fused with a [Gly Gly Gly] linker to the N-terminus or C-terminus of FliN. Three internal fusions also were constructed. Locations were chosen by considering the known interactions between FliN, FliM and FliG, and by inspection of the primary, secondary and tertiary structure of FliN. The [linker][YFP][linker] insertion [Gly Gly Gly][YFP_{Ser}…YFP_{Lys}][Ser Gly Gly Gly Gly] was placed between FliN codons 45 and 46, 93 and 94, and 115 and 116 (the notation used here labels the N-terminal methionine as codon 1). Cells carrying a genomic *fliN* deletion and expressing the N-terminal fusion (YFP-FliN) or the internal fusion between codons 45 and 46 (FliN-YFP_{INT}) were motile and fluorescent. The other fusions did not rescue *fliN* function in a Δ*fliN* background. These results can be understood in the context of a FliN docking model where a FliN tetramer forms a torus, with C-termini pointing into the hole and N-termini facing out[15].

We tested the functional fusions for tethered-cell rotation and fluorescence localization using Total Internal Reflection Fluorescence (TIRF) microscopy. Results are shown in Table 1. YFP-FliN motors rotated more slowly and were much dimmer than FliN-YFP_{INT} motors, and were also defective for switching (CW bias = 0). The functionality of FliN-YFP_{INT} motors was similar to parent strain (RP437) motors containing WT FliN. (We note that our RP437 rotation statistics are similar to previous measurements[16] but dissimilar to those of AW405[17]). Furthermore, FliM-YFP motors had an intensity relative to that of FliN-YFP_{INT}

motors of 0.20±0.11, consistent with the expected FliM:FliN stoichiometry of ~1:4[5]. We chose to proceed in our investigation using FliN-YFP$_{INT}$.

Kinetic Model

The model developed here for the interpretation of our results in later sections is based on previous work[10,12]. The model describes the subunit kinetics of steady-state and adapting motors, accounting for exchanging and non-exchanging fractions, and including the effects of bleaching of subunits in both the motor and cytoplasm.

The total number of subunits in the motor is $N(t) = N_T + N_W(t)$, where $N_T(t)$ is the number of tightly bound (non-exchanging) subunits, $N_W(t)$ is the number of weakly bound (exchanging) subunits, and t is time. Rates of change are:

$$\frac{dN_W(t)}{dt} = (B - N_W(t))\, Uk_{\text{on}} - N_W(t)\, k_{\text{off}} \quad \text{(eq1)}$$

$$\frac{dN_T(t)}{dt} = 0 \quad \text{(eq2)}$$

where B is the total number of weak binding sites, U is the number of subunits in the cytoplasm, k_{on} is the subunit on-rate, and k_{off} is the subunit off-rate. We define the pseudo on-rate Uk_{on}. For motors at steady-state, eq1 gives:

$$(B - EN)\, Uk_{\text{on}} = ENk_{\text{off}} \quad \text{(eq3)}$$

where N is the steady-state number of subunits in the motor and E is the fraction of motor subunits undergoing exchange.

The number of fluorescent subunits in the motor is $F(t) = F_T(t) + F_W(t)$, where $F_T(t)$ is the number of fluorescent tightly bound subunits and $F_W(t)$ is the number of fluorescent weakly bound subunits. Rates of change are:

$$\frac{dF_W(t)}{dt} = (B - N_W(t))\, L(t)\, k_{\text{on}} - F_W(t)\, k_{\text{off}} - \lambda_1 F_W(t) \quad \text{(eq4)}$$

$$\frac{dF_T(t)}{dt} = -\lambda_1 F_T(t) \quad \text{(eq5)}$$

where λ_1 is the fluorescence bleaching rate of subunits in the motor, and $L(t)$ is the number of fluorescent subunits in the cytoplasm, with rate of change:

$$\frac{dL(t)}{dt} = -\lambda_2 L(t) \quad \text{(eq6)}$$

where λ_2 is the fluorescence bleaching rate of subunits in the cytoplasm. We do not consider rates of change in space - we assume the intervals between exposures in our experiments are

large enough that cytoplasmic fluorescence becomes uniform. For motors at steady-state, eq4 becomes

$$\frac{dF_W(t)}{dt} = ENk_{\text{off}}\frac{L(t)}{U} - F_W(t)\,k_{\text{off}} - \lambda_1 F_W(t) \quad \text{(eq7)}$$

FliN-YFP$_{INT}$ exchange kinetics

Previous studies have used Fluorescence Recovery After Photobleaching (FRAP) to investigate the exchange kinetics of FliM fluorescent fusions[11–13]. The motor at the centre of rotation of a tethered cell can be bleached with a high-intensity pulse[11] or a TIRF field[12]. Motor fluorescence recovers as bleached subunits in the motor exchange with fluorescent subunits in the cytoplasm. Fig. 1A illustrates a FRAP experiment on a motor containing FliN-YFP$_{INT}$. The apparent recovery (~30% in ~15 min) is much greater than observed in previous work (~10% in ~1 hr)[13], and indicates appreciable exchange of FliN-YFP$_{INT}$ between motor and cytoplasm.

Lele *et al*.[12] identified the rotational state as an important factor when considering FliM-YFP exchange. We overexpressed CheY to measure recoveries in CW motors and used a *cheY* deletion strain to measure recoveries in CCW motors. To quantify the kinetics of exchange we measured recovery as a function of time. FRAP experiments were conducted as described in Fig. 1A, but with a wait interval of either 1, 2, 4, 5, 7, 10 or 15 min. The theoretical time-course of recovery is obtained by solving eq5 and eq7 for post-bleach conditions $F_T(t) = 0$, $F_W(0) = 0$, $\lambda_1 = 0$, and $L(t) = \alpha U$ (where α is the fraction of subunits in the cytoplasm that are fluorescent). The relative recovery is:

$$\frac{F(t)}{N} = \alpha E\left(1 - e^{-k_{\text{off}}t}\right) \quad \text{(eq8)}$$

For our setup, the relative cytoplasmic fluorescence after bleaching was previously measured to be 0.7[12]. We divide experimental recoveries by $\alpha = 0.7$ and fit the time-courses with eq8/α to obtain exchanging fractions and off-rates. Time-courses for CW and CCW motors are shown in Figs. 1B and C. For FliM-YFP, the exchanging fraction in CW motors (0.63±0.02) is higher than the exchanging fraction in CCW motors (0.24±0.01) and the off-rate is independent of rotation direction (0.024±0.003 s^{-1} for CW rotation and 0.019±0.005 s^{-1} for CCW rotation)[12]. Except for the magnitude of the off-rate, the details of exchange for FliN-YFP$_{INT}$ are similar: the exchanging fraction in CW motors (0.53±0.12) is greater than the exchanging fraction in CCW motors (0.32±0.05) and the off-rate is independent of rotation direction (0.004±0.002 s^{-1} for CW rotation and 0.005±0.002 s^{-1} for CCW rotation). The FliN-YFP$_{INT}$ off-rate is ~4-5 times lower than the FliM-YFP off-rate.

These data demonstrate that, like FliM-YFP, the population of FliN-YFP$_{INT}$ in the motor is divided between subunits that are tightly bound (non-exchanging) and subunits that are weakly bound (exchanging), and that the tightly bound fraction is larger in the CCW state. The independence of off-rate on rotation direction demonstrates that off-rate does not play a role in remodelling, contradicting the suggestion of an earlier study[10]. For FliM-YFP, the

difference in tightly bound fractions results in CCW motors hosting more FliM-YFP subunits than CW motors[12]. This difference in stoichiometry forms the basis of adaptation. We proceed to investigate the stoichiometry of FliN-YFP$_{INT}$.

FliN-YFP$_{INT}$ stoichiometry

We measured FliN-YFP$_{INT}$ motor intensity with TIRF as a function of [CheY-P] to explore FliN-YFP$_{INT}$ stoichiometry (Fig. 2A). The variation in the FliN-YFP$_{INT}$ motor intensity matches the variation in FliMYFP motor intensity, demonstrating that the ratio of the proteins in the motor remains constant. As reported for FliM-YFP motors[12], FliN-YFP$_{INT}$ CCW motors are brighter than CW motors, indicating the presence of more subunits in the CCW state. There is no dependence of intensity on [CheY-P] per se – intensity is constant below 2 μM CheY-P and above 4 μM CheY-P – suggesting that CheY-P is not involved in the remodelling process[11].

We develop the model for CW and CCW motor stoichiometry outlined by Lele *et al.*[12]. The CW motor is known to host ~34 FliM subunits[18] and ~34 FliN tetramers[19] (our model and data cannot distinguish between monomeric or tetrameric FliN – we consider tetramers for convenience). From the measurements of relative motor intensity (Fig. 2A), the CCW motor hosts ~1.3 times as many subunits as the CW motor. Assuming proportionality between stoichiometry and fluorescence intensity, this equates to ~44 FliM subunits and ~44 FliN tetramers. The exchanging fractions determined earlier can be used to calculate the number of weakly bound and tightly bound subunits in each rotational state. When the off-rate and pseudo on-rate for weakly bound subunits are equal (which was described to be the case for CCW FliM-YFP motors[12]), the weakly bound subunits occupy half of the available binding sites (see eq3). This indicates ~55 FliM binding sites in total for the CCW motor, and by extension ~55 FliN tetramer binding sites. We assume the CW motor also has a total of ~55 binding sites. The model is visualized in Fig. 2B.

FliN-YFP$_{INT}$ adaptation kinetics

Yuan *et al.*[10] observed the real-time increase in FliM-YFP motor intensity associated with the change in stoichiometry when motors switch from CW to CCW rotation. We performed the same experiment using FliN-YFP$_{INT}$. A *cheR cheB* deletion strain was used, where motor adaptation can be observed in the absence of receptor adaptation. The *cheR cheB* strain yields motors with a wide range of biases. We selected CW motors and monitored motor intensity with TIRF (Fig. 3A). An expression for the decay is obtained by solving eqs 5,6 and 7 for initial conditions $F_W(0) = EN$, $F_T(0) = (1 - E)N$ and $L(0) = U$:

$$\frac{F(t)}{N} = E\left[\left(1 - \frac{k_{\mathrm{off}}}{\lambda_1 - \lambda_2 + k_{\mathrm{off}}}\right) e^{-(\lambda_1 + k_{\mathrm{off}})t} + \frac{k_{\mathrm{off}}}{\lambda_1 - \lambda_2 + k_{\mathrm{off}}} e^{-(\lambda_2)t}\right] + (1 - E)\, e^{-\lambda_1 t} \quad \text{(eq9)}$$

The data are fitted with eq9. Parameters are described in the figure caption. The difference between the FliM-YFP and FliN-YFP$_{INT}$ decay curves is partly due to a difference in the YFP bleaching rates (laser and exposure settings were different between the two experiments), but also due to the FliN-YFP$_{INT}$ off-rate being lower than FliM-YFP off-rate. FliN-YFP$_{INT}$ motors are not replenished with fluorescent subunits from the cytoplasm as

quickly as FliM-YFP motors. Hence, the decay in the intensity of FliN-YFP$_{INT}$ motors is greater than in FliM-YFP motors.

We repeated the above experiment, but introduced strong attractant (2mM MeAsp + 0.5 mM L-serine) after time t_a to induce CCW rotation. The results are shown in Figure 3B, together with the fits from Figure 3A for comparison. Following the switch, the rate of decay is reduced, indicating the addition of both FliM-YFP and FliN-YFP$_{INT}$ subunits. We interpret the result in terms of the model illustrated in Fig. 2B. When the switch occurs, the weakly bound subunits in the motor become tightly bound, and vacant sites begin to fill up with new, weakly bound subunits. A new steady-state is reached when ~half of these sites are occupied. A formal description is provided by solving eq1-5 with conditions $N_W(t_a) = 0$, $N_T(t_a) = N$, $F_W(t_a) = 0$, $F_T(t_a) = F(t_a)$ and the approximation $L(t_a) = U$:

$$N_W(t) = N_W\left(1 - e^{-(Uk_{on}+k_{off})(t-t_a)}\right) \quad \text{(eq10)}$$

$$\frac{F_T(t)}{N} = \frac{F(t_a)}{N} e^{-\lambda_1(t-t_a)} \quad \text{(eq11)}$$

$$\frac{F_W(t)}{N} = \frac{N_W}{N}\left[\frac{k_{off}e^{-\lambda_2(t-t_a)}}{\lambda_1 - \lambda_2 + k_{off}} - \frac{(UK_{on})\,e^{(-k_{off}+\lambda_2+Uk_{on})(t-t_a)}}{\lambda_2 - \lambda_1 + Uk_{on}} - \frac{(Uk_{on}+k_{off})(\lambda_1-\lambda_2)\,e^{-(k_{off}+\lambda_1)(t-t_a)}}{(\lambda_1-\lambda_2)(k_{off}-Uk_{on})+(\lambda_1-\lambda_2)^2 - Uk_{on}k_{off}}\right] \quad \text{(eq12)}$$

where N_W is the new steady-state number of weakly bound subunits. The sum of eq11 and eq12 describe the fluorescent signal in Fig. 3B as the motor adapts and reaches a new steady-state.

To isolate the fluorescent contribution of the new subunits from the fluorescent contribution of the old subunits, previous work[10] subtracted the CW decay from the CCW decay. However, the present model indicates that this will underestimate the fluorescent contribution of the new subunits. According to the model, all old subunits are tightly bound following the switch. Consequently, the fluorescence of the old subunits will decay at a greater rate than the CW decay, where about two-thirds of the subunits are undergoing exchange and replenishing motor fluorescence. The theoretical decay for the case that all old subunits are tightly bound (eq11) is plotted for the FliN case as a dashed line in Figure 3B. This is the decay that should be subtracted from CCW decay in order to isolate the fluorescence of the new subunits.

The fluorescent signal attributed to the new subunits is presented in Fig. 3C. The increase in motor intensity following the addition of strong attractant is evident. We fit the data with eq12. For the FliM-YFP data the fit provides values for the off-rate (0.019±0.006 s^{-1}), pseudo on-rate (0.013±0.002 s^{-1}) and the steady-state number of weakly bound subunits (20±2). We note that the off-rate agrees with the value obtained in FRAP experiments[12], and that the pseudo on-rate is similar to the off-rate, as concluded before. For the FliN-YFP$_{INT}$ data, a free parameter fit could not be achieved with confidence. Given the longer timescale associated with FliN-YFP$_{INT}$ kinetics, a longer recording time might be required to obtain a dataset that can be fitted. We conducted a parameter space search (Fig. 3C, inset). For values

of the off-rate close to the value determined in the FRAP experiment, acceptable fits to the data are achieved with a pseudo on-rate in the range 0-0.004 s^{-1} and steady-state values of the number of weakly bound tetramers greater than 26. The particular fit shown in Fig. 3C is with pseudo on-rate, off-rate and steady-state values of 0.004 s^{-1}, 0.007 s^{-1} and 27 tetramers, respectively. As with FliM-YFP, the pseudo on-rate and off-rate are the same order of magnitude.

Motor adaptation has been investigated in WT motors[10]: using a bead assay, motors with high CW bias were selected and bias was monitored following the addition of weak attractant (1 mM MeAsp). The CW bias dropped to a lower value and then partially recovered (Fig. 3D, grey curve). The rate of adaptation is obtained by fitting the recovery with A(1-exp(−Bt)). For WT motors, the rate of adaptation is 0.018±0.002 s^{-1}. The number of weakly-bound subunits in the motor as a function of time during adaptation is given by eq10. The rate of remodelling is $k_{off} + Uk_{on}$. For FliM-YFP, the rate of remodelling is ~0.04 s^{-1}. For FliN-YFP_{INT} the rate of remodelling is less than 0.009 s^{-1} - less than half the rate of adaptation. If FliN is involved in adaptation, we would expect the rate of remodelling to be at least as great as the rate of adaptation. It is possible that the presence of YFP_{INT} slows down FliN kinetics. We measured adaptation in FliN-YFP_{INT} motors (Fig. 3D, black curve). The rate of adaptation was 0.008±0.002 s^{-1}, indicating that adaptation was rate-limited by FliN-YFP_{INT} remodelling. This suggests an active role for FliN in adaptation, and that FliN kinetics may be faster in the absence of YFP_{INT}.

Discussion

This study extends our understanding of motor adaptation, demonstrating that the whole base of the motor undergoes remodelling. Motors contain an exchanging and non-exchanging population of FliM and FliN subunits. The fraction of non-exchanging subunits changes with rotational state, resulting in changes in stoichiometry and, consequently, changes in sensitivity to CheY-P. The behaviour of FliM and FliN are separated only by timescale. The faster timescale of FliM would indicate that this protein is the key player in motor adaptation, but our data show that the presence of YFP_{INT} perturbs adaptation and might be slowing down FliN kinetics. Indeed, results appear to be dependent on the particulars of the fluorescent fusion: Fukuoka *et al*. reported much less exchange using GFP-FliN[13]. In light of this, it might be worth re-visiting the statement that FliG does not undergo exchange[13,14].

The defining parameters of our model for motor remodelling are listed in Table 2. Values for subunit pseudo on-rate and total number of binding sites in the CW state are missing; these can be determined by conducting the experiments of Figure 3A and B, but on motors switching from CCW to CW rotation. In contrast to the traditional view of a packed protein ring, the model describes a switch complex with an excess of binding sites, with gaps permitted between proteins in the FliM and FliN architecture. In this sense, the architecture does not need to grow or shrink to accommodate more or fewer units during adaptation. Gaps in the FliM and FliN architecture would not necessarily interfere with the act of switching. A consideration of the MWC model indicates the need to energetically decouple the binding element of the complex from the switching element of the complex[12]. In this

context, FliM and FliN may serve simply as CheY-P receptors that relay occupancy information to the intact, bistable FliG ring. Recent studies describe inner and outer FliM (and by extension, FliN) binding sites on FliG[20,21], where the inner and outer locations correspond to tightly and weakly binding sites, respectively. With 26-34 FliG subunits per motor[22,23], this scheme could account for the excess of binding sites.

These arguments apply to CW and CCW motors. In Fig. 2A, we note that the brightest motors are found in the range 0 < CW bias < 1, i.e. for motors that switch. Based on the relative intensity, the number of units in low CW bias motors is ~58. Interestingly, this is similar to the steady state number of units estimated from our adaptation experiments (Fig. 3C), after motors transitioned from the CW or high CW bias state to the CCW state. Remodelling might be enhanced in motors that switch. Further investigation is required to determine whether the observed relationship between stoichiometry and bias (Fig. 2A) is physiologically accurate or a consequence of the fusion. The exact relationship will provide information about the dynamic range of motor operation and also the precision of motor adaptation. In our data, brightness reduces with increasing CW bias, but the resolution is not sufficient to draw conclusions about whether the relationship is non-linear, as predicted by a recent model describing precise motor adaptation[24].

Methods

Strains and plasmids

For motility tests, FliN fluorescent fusions were cloned separately into pTrc99A[25] under an isopropyl-β-D-thiogalactoside (IPTG)-inducible promoter. The *fliN* deletion strain DFB223[26] was transformed separately with each construct. For tethered assay tests, DFB223 was deleted for *fliC* and transformed with pKAF131 carrying the sticky *fliC* allele under control of the native *fliC* promoter[27]. This strain was transformed separately with the constructs carrying *yfp-fliN* and *fliN-yfp*$_{INT}$. Induction was with 50 mM IPTG to yield WT levels of FliN. FliM-YFP motor data came from our previous study[10].

For CCW motor FRAP experiments, we replaced WT *fliN* in VS124 (*cheB cheZ cheY*)[28] with *fliN-yfp*$_{INT}$. All gene replacements in this investigation were with the lambda Red protocol[29]. For CW motor FRAP experiments, we transformed the CCW motor strain with pWB5, a gift from B. Wang carrying *cheY* on a pTrc99A vector and overexpressed CheY. Induction was with 100 μM IPTG. Due to the deletion of *cheB* and *cheZ*, the CheY pool in these strains is almost completely phosphorylated[4].

In FliN stoichiometry experiments, the ‘CCW (0 μM CheY-P)’ dataset was collected with the CCW motor strain above. The ‘CCW (<2 μM CheY-P)’ dataset was collected from the CW motor strain above with 0 μM IPTG -- [CheY-P] is greater than zero due to background expression from the plasmid, but less than 2 μM based on the CW bias vs [CheY-P] relationship[4]. The ‘Low/Mid/High CW bias’ datasets were collected with the CCW motor strain transformed with pVS7, a gift from V. Sourjik carrying *cheY* on a pBAD18-Kan vector[30]. Induction with 0-0.001% arabinose provided motors with 0 < CW bias ≤ 1. Motors with CW bias = 1 contributed to the CW (>4 μM CheY-P) dataset -- [CheY-P] > 4 μM based on the CW bias vs [CheY-P] relationship[4]. The ‘CW (6.85/9.7 μM CheY-P)’ datasets were

collected with the CW motor strain above induced with 30/50 μM IPTG. [CheY-P] values are from the calibration curve in reference 31.

For adaptation experiments we replaced *fliN* in JY35 (*cheR cheB fliC*)[10] with *fliN-yfp*$_{INT}$. For bead assay adaptation experiments, we transformed this strain with pKAF131.

Assays

Cells were grown at 33 °C in 10ml T-broth (1% tryptone, 0.5% NaCl) supplemented with the appropriate antibiotics (ampicillin: 100 μg ml^{-1}, kanamycin: 50 μg ml^{-1}) and inducers to an OD_{600} of 0.5. Cells with filaments were sheared to truncate flagella by passing ~1 mL of culture 50 times between two syringes with 23-gauge needles connected by polyethylene tubing. Cells were collected by centrifugation (2 min at 4000g), washed twice in 1 ml of motility medium (10 mM potassium phosphate, 0.1 mM EDTA, 10 mM lactate, pH 7.0) and resuspended in 0.2 mL motility medium. Cells were incubated with the appropriate antibody (anti-FlgE or anti-FliC, at ~0.5 μg ml^{-1}) for 20 min, washed twice in 0.3 mL of motility medium and resuspended in 0.2 mL motility medium. Antibodies were purified from antiserum using Protein A sepharose CL-4B beads (Amersham Biosciences) and a Bio Rad #731-1550 10 mL chromatographic column. Dialysis was carried out with #66810 10000 MWCO Slide-A-Lyzer dialysis cassettes (Pierce Biotechnology). Purified antibody was preadsorbed using hookless strain HCB137.

Cell suspension was flowed into a custom tunnel slide for FRAP and stoichiometry experiments, and a custom flow slide for adaptation experiments. The suspension was left for 15 min to allow cell tethering and then the chamber was rinsed with motility medium. For adaptation experiments with the bead assay, 0.01% poly-L-lysine solution (Sigma) was flowed into a custom flow slide and left for 1 min to allow coating of the coverslip, followed by rinsing. Cell suspension was flowed in and left for 15 min, followed by rinsing. A 1.0-μm polystyrene bead suspension (Polysciences) was flowed in and left for 10 min to allow attachment to sheared flagella, followed by rinsing. In adaptation experiments, the chamber was kept under constant flow (60 μL min^{-1} for tethered assays or 400 μL min^{-1} for bead assays) by syringe pump (Harvard apparatus), with either motility medium or attractant medium.

Microscopy

For TIRF work, a 25 mW Cobolt Fandango diode-pumped solid-state laser provided 515 nm light. The laser beam was gated on and off with a shutter (Vincent Associates LS6-ZM-1 with VMM-D1 driver). A fiber port (Thorlabs PAF-X-5-A) and fiber (Oz Optical QSMJ-3AF3U-488-3.5/125-3AS-3") coupled the excitation light into a Nikon TI-TIRF TIRF/Epi-fl Illuminator unit fitted on a Nikon Eclipse TI-U inverted microscope. Excitation light passed through a Z514/10 bandpass filter and was reflected by a ZT514RDC dichroic into a Nikon CFI Apo 60× 1.49 oil TIRF objective. All dichroics and filters were from Chroma Technology. When focused in the middle of the back focal plane (BFP) of the objective, the laser beam exited directly upward out of the objective at ~9.5 mW. The field was an elliptical Gaussian in shape with widths at half maximum of ~165 μm and ~220 μm. Thus the field intensity was ~8 W/cm^2.

The 1/e decay depth of the TIR evanescent wave is a function of the laser angle of incidence at the coverslip/sample interface, θ. The exit-angle of the laser from the objective as a function of the position (p) of the laser focus within the objective BFP was measured with a marked prism atop the objective, in contact by Cargille DF immersion oil. A calibration curve between p and θ was constructed, accounting for differences in refractive index between oil, prism and coverslip. The 1/e decay depth, d, was set to ~100 nm using the relation $d=(\lambda/4\pi)(n_{cover}^2\sin^2\theta-n_{sample}^2)^{-1/2}$, where λ is the laser wavelength, and n_{cover} and n_{sample} are the refractive indices of the coverslip and sample, respectively.

Emission light passed through the ZT514RDC dichroic and an ET520LP longpass filter, and was reflected by a T680LPXXR dichroic through a ET650sp-3p shortpass filter into a Nikon VM Lens C-4x telescope fitted to the back port of the TI-U. Imaging was with a 512×512 pixel EMCCD (Andor iXon Model DV887ECS-BV). Resolution was ~65 nm/pixel. The iXon peltier was set to −55°C and fan-cooled. Electron multiplier gain was set to 145. iXon control and acquisition was with Andor Solis software. For FRAP and stoichiometry experiments, acquisition was under ‘frame-transfer’ mode, with 70×100 ms exposures. For adaptation experiments, acquisition was under ‘kinetic’ mode, with 200 ms exposures every 5 s for 60 exposures. For synchronization of laser excitation and exposures, the iXon ‘shutter’ output provided input to the VMM-D1 driver. Recordings were saved as .sif files and exported as .txt files for analysis with custom Matlab scripts. Motor intensities were calculated using a Gaussian mask method, as described[10].

A Nikon TI T BPH Eyepiece tube base unit allowed for ‘external’ phase contrast microscopy. An image on the primary image plane is refocused on a secondary image plane via relay optics. This allows the TI C TPH 60x/PH4 phase ring (matching the 60x Ph4 annular ring of the Nikon CLWD 0.72 condenser) to be placed at a conjugate objective BFP instead of at the objective BFP. The result is unobstructed fluorescence microscopy. Light for external phase contrast microscopy was provided by the 100-W Ti-U halogen lamp system. After diffuser filtering, an HQ740/80 bandpass filter allowed passage of infra-red light, which passed all mentioned filters and dichroics and was imaged on a Thorlabs DCC1240M CMOS camera mounted on the TI T BPH port at the secondary image plane. Resolution was ~105 nm/pixel and at least 120 Hz. Acquisition was with custom LabView software.

Acknowledgments

We thank Pushkar Lele for input on genetic work and Junhua Yuan for useful discussions. This work was supported by National Institutes of Health Grant AI016478. M. N. S. acknowledges financial support from the Harvard Physics Department and Harvard College Program for Research in Science and Engineering.

References

1. Silverman M, Simon M. Flagellar rotation and the mechanism of bacterial motility. Nature. 1974; 249:73–4. [PubMed: 4598030]
2. Larsen SH, Reader RW, Kort EN, Tso WW, Adler J. Change in direction of flagellar rotation is the basis of the chemotactic response in Escherichia coli. Nature. 1974; 249:74–7. [PubMed: 4598031]
3. Berg HC. Dynamic properties of bacterial flagellar motors. Nature. 1974; 249:77–9. [PubMed: 4598032]

4. Cluzel P, Surette M, Leibler S. An ultrasensitive bacterial motor revealed by monitoring signaling proteins in single cells. Science. 2000; 287:1652–5. [PubMed: 10698740]
5. Brown PN, Terrazas M, Paul K, Blair DF. Mutational analysis of the flagellar protein FliG: sites of interaction with FliM and implications for organization of the switch complex. J. Bacteriol. 2007; 189:305–12. [PubMed: 17085573]
6. Zhou J, Lloyd SA, Blair DF. Electrostatic interactions between rotor and stator in the bacterial flagellar motor. Proc. Natl. Acad. Sci. 1998; 95:6436–6441. [PubMed: 9600984]
7. Bren A, Eisenbach M. The N terminus of the flagellar switch protein, FliM, is the binding domain for the chemotactic response regulator, CheY. J. Mol. Biol. 1998; 278:507–14. [PubMed: 9600834]
8. Sarkar MK, Paul K, Blair D. Chemotaxis signaling protein CheY binds to the rotor protein FliN to control the direction of flagellar rotation in Escherichia coli. Proc. Natl. Acad. Sci. U. S. A. 2010; 107:9370–5. [PubMed: 20439729]
9. Dyer CM, Vartanian AS, Zhou H, Dahlquist FW. A molecular mechanism of bacterial flagellar motor switching. J. Mol. Biol. 2009; 388:71–84. [PubMed: 19358329]
10. Yuan J, Branch RW, Hosu BG, Berg HC. Adaptation at the output of the chemotaxis signalling pathway. Nature. 2012; 484:233–6. [PubMed: 22498629]
11. Delalez NJ, Wadhams GH, Rosser G, Xue Q, Brown MT, Dobbie IM, Berry RM, Leake MC, Armitage JP. Signal-dependent turnover of the bacterial flagellar switch protein FliM. Proc. Natl. Acad. Sci. U. S. A. 2010; 107:11347–51. [PubMed: 20498085]
12. Lele PP, Branch RW, Nathan VSJ, Berg HC. Mechanism for adaptive remodeling of the bacterial flagellar switch. Proc. Natl. Acad. Sci. U. S. A. 2012; 109:20018–22. [PubMed: 23169659]
13. Fukuoka H, Inoue Y, Terasawa S, Takahashi H, Ishijima A. Exchange of rotor components in functioning bacterial flagellar motor. Biochem. Biophys. Res. Commun. 2010; 394:130–5. [PubMed: 20184859]
14. Li H, Sourjik V. Assembly and stability of flagellar motor in Escherichia coli. Mol. Microbiol. 2011; 80:886–99. [PubMed: 21244534]
15. Sowa Y, Berry RM. Bacterial flagellar motor. Q. Rev. Biophys. 2008; 41:103–32. [PubMed: 18812014]
16. Lapidus IR, Welch M, Eisenbach M. Pausing of flagellar rotation is a component of bacterial motility and chemotaxis. J. Bacteriol. 1988; 170:3627–32. [PubMed: 3042756]
17. Berg HC, Tedesco PM. Transient response to chemotactic stimuli in Escherichia coli. Proc. Natl. Acad. Sci. U. S. A. 1975; 72:3235–9. [PubMed: 1103143]
18. Thomas DR, Francis NR, Xu C, DeRosier DJ. The three-dimensional structure of the flagellar rotor from a clockwise-locked mutant of Salmonella enterica serovar Typhimurium. J. Bacteriol. 2006; 188:7039–48. [PubMed: 17015643]
19. Zhao R, Pathak N, Jaffe H, Reese TS, Khan S. FliN is a major structural protein of the C-ring in the Salmonella typhimurium flagellar basal body. J. Mol. Biol. 1996; 261:195–208. [PubMed: 8757287]
20. Passmore SE, Meas R, Marykwas DL. Analysis of the FliM/FliG motor protein interaction by two-hybrid mutation suppression analysis. Microbiology. 2008; 154:714–24. [PubMed: 18310018]
21. Paul K, Brunstetter D, Titen S, Blair DF. A molecular mechanism of direction switching in the flagellar motor of Escherichia coli. Proc. Natl. Acad. Sci. U. S. A. 2011; 108:17171–6. [PubMed: 21969567]
22. Lee LK, Ginsburg MA, Crovace C, Donohoe M, Stock D. Structure of the torque ring of the flagellar motor and the molecular basis for rotational switching. Nature. 2010; 466:996–1000. [PubMed: 20676082]
23. Paul K, Gonzalez-Bonet G, Bilwes AM, Crane BR, Blair D. Architecture of the flagellar rotor. EMBO J. 2011; 30:2962–71. [PubMed: 21673656]
24. Tu Y, Berg HC. Tandem adaptation with a common design in Escherichia coli chemotaxis. J. Mol. Biol. 2012; 423:782–8. [PubMed: 22922485]
25. Amann E, Ochs B, Abel KJ. Tightly regulated tac promoter vectors useful for the expression of unfused and fused proteins in Escherichia coli. Gene. 1988; 69:301–315. [PubMed: 3069586]

26. Tang H, Billings S, Wang X, Sharp L, Blair DF. Regulated underexpression and overexpression of the FliN protein of Escherichia coli and evidence for an interaction between FliN and FliM in the flagellar motor. J. Bacteriol. 1995; 177:3496–3503. [PubMed: 7768859]

27. Yuan J, Fahrner KA, Turner L, Berg HC. Asymmetry in the clockwise and counterclockwise rotation of the bacterial flagellar motor. Proc. Natl. Acad. Sci. U. S. A. 2010; 107:12846–12849. [PubMed: 20615986]

28. Sourjik V, Berg HC. Receptor sensitivity in bacterial chemotaxis. Proc. Natl. Acad. Sci. U. S. A. 2002; 99:123–7. [PubMed: 11742065]

29. Datsenko KA, Wanner BL. One-step inactivation of chromosomal genes in Escherichia coli K-12 using PCR products. Proc. Natl. Acad. Sci. U. S. A. 2000; 97:6640–6645. [PubMed: 10829079]

30. Guzman LM, Belin D, Carson MJ, Beckwith J. Tight regulation, modulation, and high-level expression by vectors containing the arabinose PBAD promoter. J. Bacteriol. 1995; 177:4121–4130. [PubMed: 7608087]

31. Sourjik V, Berg HC. Binding of the Escherichia coli response regulator CheY to its target measured in vivo by fluorescence resonance energy transfer. Proc. Natl. Acad. Sci. U. S. A. 2002; 99:12669–74. [PubMed: 12232047]

Highlights

- Adaptive remodelling has been observed in rotary motors for FliM but not FliN
- Using an internal fluorescent fusion, we find that remodelling does occur with FliN
- Remodelling is enhanced by motor switching
- This work reconciles the apparent mismatch between the activities of FliM and FliN

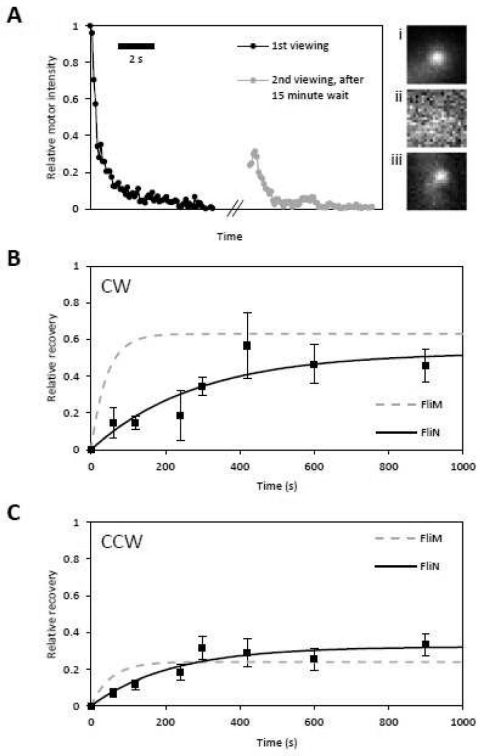

Figure 1.

FliN-YFP$_{INT}$ exchange kinetics. A) FRAP experiment on a motor containing FliN-YFP$_{INT}$. During TIRF imaging, motor fluorescence intensity decays due to photobleaching and is fit with $A_1\exp(-B_1t)+C_1$. After an interval of 15 min, the motor is imaged again and fitted with $A_2\exp(-B_2t)+C_2$. For direct comparison to the data presented in reference 12, the apparent recovery of motor fluorescence is calculated as $(A_2+C_2-C_1)/A_1 \sim 0.3$. Each viewing comprises 70×100ms exposures. Images i, ii, and iii are frames from the beginning of the first viewing, end of the first viewing, and beginning of the second viewing, respectively. Pixel values are scaled between 0 and 64 within each frame. B) Timecourse of recovery in CW motors. From left to right: sample sizes are 7, 6, 8, 5, 4, 16 and 9 motors. Black squares are means and bars are standard errors. Black curve is the fit to the data with eq8/α. The grey dashed curve is the fit to CW FliM-YFP motor data, reproduced from Fig 2E of reference 12. See main text for fit parameter values ± standard errors. C) The same as (B) but with CCW motors (sample sizes are 15, 15, 8, 11, 8, 15 and 15 motors).

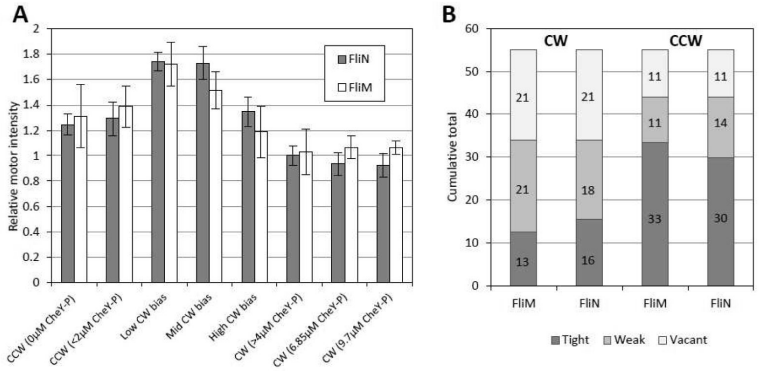

Figure 2.

FliN-YFP$_{INT}$ stoichiometry. (A) Relative motor intensity as a function of [CheY-P]. See Methods for estimation of [CheY-P]. Low bias motors have 0 < CW bias <= 0.33, mid bias motors have 0.33 < CW bias <= 0.66 and high bias motors have 0 < CW bias < 0.33. FliN motor intensity curves were fitted with Aexp(−Bt)+C and motor intensity was calculated as A+C. FliM-YFP values were calculated from the datasets used to produce figures 1C and 1D in reference 12. From left to right: FliN-YFP$_{INT}$ sample sizes are 29, 20, 13, 19, 17, 25, 25 and 23; FliM-YFP sample sizes are 63, 4, 6, 10, 10, 6, 19 and 28. Bar heights are means and error bars are standard errors. FliN-YFP$_{INT}$ motor intensities are relative to the 'CW (>4 μM CheY-P)' dataset. FliM-YFP motor intensities are relative to the CW mutant dataset in Figure 1D of reference 12. (B) Model for motor stoichiometry. The motor has ~55 FliM binding sites. In the CW state, ~13 of these sites are occupied by tightly bound units, and ~half of the remaining sites are occupied by weakly bound units. In the CCW state, ~33 of the sites are occupied by tightly bound units and ~half of the remaining sites are occupied by weakly-bound subunits. The same model applies to FliN tetramers. Numbers of weakly and tightly bound units, along with numbers of vacant sites, are indicated on the bars.

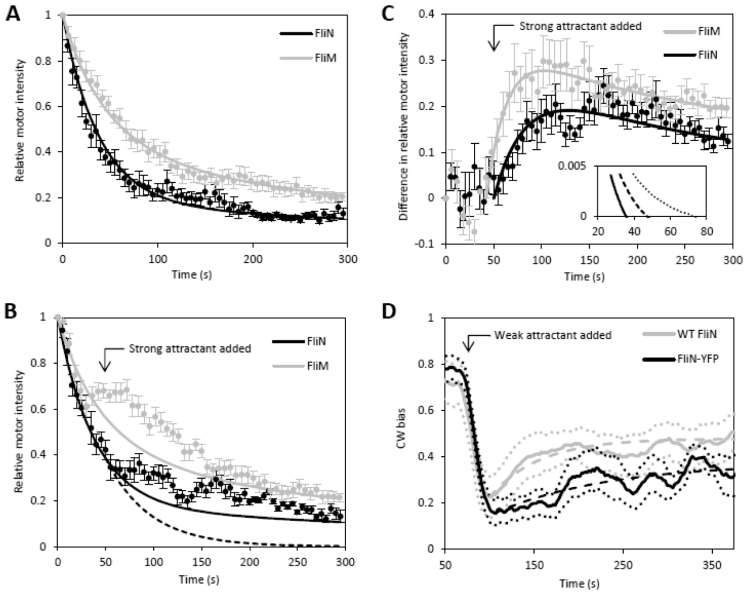

Figure 3.

FliN-YFP$_{INT}$ adaptation kinetics. (A) Relative intensity of CW FliN-YFP$_{INT}$ motors and high CW bias FliM-YFP motors (reproduced from Fig. 4C of reference 10) as a function of time. The relative intensities of 8 FliN-YFP$_{INT}$ motors were averaged. Circles are means and bars are standard errors. Curves are fits to the data with eq9. The data do not constrain fitting of all parameters. We allowed the exchanging fractions and off-rates to vary within the 95% confidence bounds determined in the FRAP experiments and fitted for bleaching rates. Final values for FliM-YFP and FliN-YFP$_{INT}$ exchanging fractions were 0.59 (95% confidence lower bound) and 0.77 (95% confidence upper bound), respectively; final values for off-rates were 0.018 s^{-1} (95% confidence lower bound) and 0.007 s^{-1} (95% confidence upper bound), respectively; final values for motor bleaching rates were 0.015±0.0002 s^{-1} and 0.024±0.0004 s^{-1}, respectively; final values for cytoplasmic bleaching rates were 0.0021±0.0002 s^{-1} and 0.0018±0.0006 s^{-1}, respectively. We note that these values are consistent with the cytoplasmic bleaching rate calculated from α=0.7=exp($-\lambda_2 t$), once scaled for the difference in exposure rate between our experiment and the experiment in (12). (B) Relative intensities during motor adaptation. The relative intensities of 8 FliN-YFP$_{INT}$ motors were averaged. Circles are means and bars are standard errors. FliM-YFP motor data is from reference 10. A switch from CW to CCW rotation was induced at $t_a \approx 50$ s in FliN-YFP$_{INT}$ experiments. A switch from high CW bias rotation to CCW rotation was induced at $t_a \approx 42$ s in FliM-YFP experiments. Solid curves are fits from A, plotted for comparison. Dashed curve is eq11. (C) Data in B re-plotted to show fluorescent signal of additional subunits. Curves are fits to the data with eq12. The value of N in eq12 was 41 for the fit to FliM data, and 34×4 for the fit to FliN data (values based on data in Figure 2A).See main text for fit parameter values. Inset: parameter space search. Abscissa is steady-state weakly bound number of tetramers, ordinate is fitted pseudo on-rate. Off-rate was either 0.003 s^{-1} (dotted line), 0.005 s^{-1} (dashed line) or 0.007 s^{-1} (solid line), consistent with the FRAP experiment off-rate 0.005±0.002 s^{-1}. Only parameter sets resulting in fits with R-squared>0.7 are plotted. (D) Partial recovery of bias in *cheR cheB* cells after the addition of

weak attractant. Solid lines are means, dotted lines are means ± standard errors. Dashed lines are fits to the data with A(1-exp(−Bt)). WT motor data is reproduced from reference 10. FliN-YFP_{INT} sample size is 5 motors.

Table 1

Properties of motors containing either YFP-FliN, FliN-YFP_{INT} or WT FliN. Numbers are mean ± standard error.

	YFP-FliN (n=9)	FliN-YFPINT (n=10)	WT FliN (n=13)
CCW rotation rate (Hz)	2.36±1.02	5.40±2.24	5.60±1.80
CW bias	0.00±0.00	0.02±0.04	0.04±0.08
Relative brightness	0.23±0.03 (n=11)	1±0.10 (n=11)	n/a

Table 2

Defining parameters of the kinetic and stoichiometric models. Numbers are mean ± standard error.

	FliM-YFP		FliN-YFP$|_N$T		
Parameter	**CW**	**CCW**	**CW**	**CCW**	**Reference**
N	34	~44	~4×34	~4×44	12, 17, this work
E	0.63±0.02	0.24±0.01	0.53±0.12	0.32±0.05	12, this work
^{k} off $^{(s}$)	0.024±0.003	0.019±0.005	0.004±0.002	0.005±0.002	12, this work
Ukon (s'^{1})	-	0.013±0.002	-	0-0.004	10, this work
binding sites	-	~55	-	~4×55	12, this work